ELSEVIER

Chemical Engineering Journal 142 (2008) 109–121

Chemical Engineering Journal

www.elsevier.com/locate/cej

Design and characterisation of the staggered herringbone mixer

Suet Ping Kee, Asterios Gavriilidis *

Department of Chemical Engineering, University College London, Torrington Place, London WC1E 7JE, United Kingdom

Received 11 December 2007; accepted 4 February 2008

Abstract

The staggered herringbone mixer was studied using computational fluid dynamics (CFD) and particle tracking methods. The positions of tracer particles as well as the stretching of a fluid element associated with each tracer particle were tracked using a fourth order Runge-Kutta integration scheme with adaptive time stepping. Striation patterns observed were in qualitative agreement with experimental work from literature. The computed stretch values were found to be log-normally distributed. The specific stretch per period for a spatially periodic flow was computed. This allows for an estimation of the required length for complete mixing by further accounting the penetration depth achieved by molecular diffusion. The microchannel lengths for complete mixing computed using the mean stretch were lower than those obtained experimentally. This was attributed mainly to the fact that the experimentally derived values were measured in the central 50% of the mixer cross-section where striation thickness reduction can be observed to be slower. Furthermore, the specific stretch per period represents the mean stretch value while in reality the stretch values are distributed log-normally. In the design of mixers, a conservative estimate of the required mixing length can be obtained by replacing the mean stretch per period with a value which represents the cut-off point for the lower 10% of the distribution. The design lengths computed using these values were slightly higher than experimental ones and found to exhibit the same trend with increasing Peclet number. The pressure drop at various *Re* was also investigated and was found to be slightly lower than that of an equivalent grooveless channel.

Keywords: Micromixer; Staggered herringbone mixer; Chaotic micromixer

1. Introduction

In recent years, microfluidic systems have gained widespread applications in a number of fields such as analytical chemistry, high-throughput synthesis and microchemical processing. One aspect of microfluidic systems that has attracted considerable interest is the mixing of fluids in miniaturized systems. Fluid flows in miniaturized systems are characterized by low values of Reynolds number ($Re = \rho ud/\mu$). At low-*Re* number, the flow is laminar and mixing occurs only by molecular diffusion. The characteristic length scales in microfluidic applications are frequently of the order of several hundred microns, which allow rapid mixing by molecular diffusion alone. Examples of such mixers include the T-type and Y-type micromixers [1,2]. However, in cases where the molecular diffusivity is very low (in biotechnology applications for example, molecular diffusivity for proteins are typically around 10^{-11} m^2/s), mixing by molecular diffusion becomes very slow, requiring lengths of up to several metres for complete mixing to occur. Various micromixer designs have been reported in the literature. These include various flow lamination mixers such as interdigital micromixers [3–5], split and recombine mixers [6], geometric focusing mixers [3–5,7], secondary flow micromixers [8] and chaotic mixers [9–11]. Detailed reviews of the various types of micromixers are available elsewhere [12–15].

Chaotic micromixers, where the fluid volumes are stretched and folded over the cross-section of the channel, are particularly effective for reducing the mixing length. The stretching and folding of fluid volumes proceed exponentially as a function of the axial distance travelled, accelerating mass transfer by increasing the interfacial area and decreasing the striation thickness over which diffusion must occur for complete homogenization. One of the earliest reports on chaotic micromixers was based on placing microstructured objects within the flow passage on one side of the microchannel walls. Bas-relief structures, such as oblique ridges and staggered herringbones on the floor of channels were used to induce steady chaotic flows in the slanted groove [16] and staggered herringbone micromixers, respectively [17]. The staggered herringbone offered superior mixing performance at low *Re* numbers, low resistance to flow

* Corresponding author. Tel.: +44 20 76793811; fax: +44 20 73832348.
E-mail address: a.gavriilidis@ucl.ac.uk (A. Gavriilidis).

1385-8947/$ – see front matter © 2008 Elsevier B.V. All rights reserved.
doi:10.1016/j.cej.2008.02.001

Nomenclature

a	ratio of the groove half height to the channel height
A	COV of unmixed inlet stream, see (6)
B	rate of decrease of the COV, see (6)
COV	coefficient of variance
d	characteristic length (m)
d_E	channel equivalent diameter (m)
D	diffusion coefficient (m^2/s)
h	channel height (m)
H_n	normalised helicity
$\boldsymbol{l}$	fluid filament vector tracked for stretching computations
$\boldsymbol{l_0}$	initial condition for vector $\boldsymbol{l}$
L	length (m)
L_{cycle}	length per mixing cycle (m)
m	mean
n	mixing cycle number
n_{mix}	number of cycles for complete mixing
n_{90}	required number of mixing cycles computed using α_{90} values
N	number of particles
N_i	number of particles cell i
N_T	total number of particles within the grid
N_{T0}	initial number of tracked particles
$\bar{N}$	average particle concentration per cell
p	degree of asymmetry of herringbone grooves
Pe	Peclet number
ΔP	pressure drop (Pa)
q	Groove wave vector
Q	volumetric flow (m^3)
Re	Reynolds number
$s(0)$	striation thickness at time = 0 (μm)
$s(n)$	striation thickness after n cycles (μm)
S	Shannon entropy (bits)
t	time (s)
u	velocity (m/s)
$\bar{u}$	average velocity (m/s)
$\boldsymbol{v}(\boldsymbol{x})$	particle velocity as a function of position (m/s)
$(\nabla \boldsymbol{v})^T$	velocity gradient tensor (s^{-1})
w	channel width (μm)
$\boldsymbol{x}$	vector of particle position
y	mixing length (m)
y_{dif}	diffusional mixing length (m)
y_{50}	mixing length computed from α_{50} (m)
y_{90}	mixing length computed from α_{90} (m)

Greek letters

α	stretching function
α_{50}	stretch per period (based on $\lambda_{g,50}$ values)
α_{90}	stretch per period (based on $\lambda_{g,90}$ values
δ	Lyapunov exponent (s^{-1})
δ_x	penetration distance (m)
θ	Groove angle (°)
λ	stretching experienced by vector $\boldsymbol{l}$, see (3)
$\lambda_{g,50}$	geometric mean stretch over all vectors on a given cross-section
$\lambda_{g,90}$	cut-off point of the distribution of stretch values where 90% of stretch values are higher (see Fig. 9)
μ	viscosity (Pa s)
ρ	density (kg/m^3)
σ	standard deviation
σ^2	variance (number based)
τ	average residence time per mixing cycle (s)
φ	mass fraction

and is relatively easy to fabricate using planar lithographic methods. It was found to work well for Reynolds numbers from 1 to 100 and for Peclet numbers of up to 1×10^6, with the required mixing length increasing only logarithmically with the Peclet number.

The flow patterns in bas-relief structured channels have been studied extensively. A number of numerical studies have been carried out on grooved microchannel mixers which considered the effects of various geometric parameters on mixing performance. Many of the numerical approaches used for characterising mixing performance are based on methods used for macro-scale static mixers such as the coefficient of variance, intensity of segregation, stretching histories, Poincaré sections, rate of strain tensor, number of striations and residence time distributions [18–20]. Wang et al. [21] evaluated the slanted groove micromixer using a computational fluid dynamics (CFD) package to simulate the 3D velocity field for particle tracking purposes as well as to study two-fluid mixing. Streaklines from slanted groove microchannels twist in a helical shape, indicating folding and stretching of fluids. Poincaré maps were generated by advecting one or a series of passive particles through a series of periodic planes located at the end of each mixing segment and each position of the particle which hits this plane was then recorded. The Poincaré map obtained indicated an increase in flow irregularity on increasing the groove aspect ratio, with particle trajectories circling around the flow axis. By counting the dots per circle in the Poincaré map, the length required for one complete recirculation was computed, which was then used as a basis for evaluating mixing performance. The length required for one complete recirculation decreased exponentially with increasing groove aspect ratio. The mean helicity, measured from the angle between the longitudinal channel axis and the interfacial line of two fluid streams shifted by the helical flow pattern, was found to be independent of flow velocity and was a function of geometric parameters only, especially the aspect ratio of grooves. Schönfeld and Hardt [22] simulated the helical flows produced in the slanted groove micromixer. The relative transverse velocities as a function of the vertical position were evaluated and found to be in good agreement with experimental results [23]. Double-sided structured channels were found to increase the relative transverse velocity significantly. The relative transverse velocities were also found to be independent of Reynolds number.

Aubin et al. [24] compared the flow pattern and mixing behaviour in both the slanted groove and staggered herringbone mixers using CFD and particle tracking methods. Better mixing was observed in the staggered herringbone micromixer due to the formation of two helical flows, with alternating small and large vortices rotating in opposite directions. Calculation of variance of the dispersion of particle tracers and the mean stretching of fluid filaments were found to be good methods for characterizing the mixers while the rate of strain tensor appeared not to be well adapted for the mixers studied. More recently, Aubin et al. [25] studied the effects of geometric parameters such as groove depth, number of grooves per cycle and groove width on the mixing quality. An alternative method for characterizing the mixing performance was introduced, which is based on a statistical method called nearest neighbour analysis. Mixing quality was found to improve with deeper and wider grooves, but was relatively unaffected by the number of grooves per cycle.

Simple analytical models have been derived for the flow behaviour in both slanted groove and staggered herringbone micromixers [23,26]. Poincaré maps and mixing simulations using the models indicate the existence of an optimal degree of asymmetry, p (fraction of channel width occupied by the wide arm of the herringbones) for the herringbone grooves in the interval $7/12 < p < 2/3$. For a fixed value of the ratio of transverse to axial velocity, a minimum axial length per half-cycle was required, below which mixing is poor. Yang et al. [27] presented a numerical study of the effects of geometric parameters such as depth ratio of the grooves, asymmetry index, groove intersection angle and upstream to downstream channel width ratio on the mixing performance of the staggered herringbone mixer. Two dominant mechanisms of mixing were identified; the stretching and folding of the interface due to the vertical motions of flow at the groove's side edge and the increase in contact area between the two fluids due to underside fluid transportation. The groove depth ratio and asymmetry index were found to be the most influential. Results from a pressure loss analysis indicated better mixing with higher groove flow rate, which can be achieved by decreasing the asymmetry index and increasing the depth ratio of the groove. The effect of the groove asymmetry and the number of grooves per half cycle on the mixing performance was also investigated by Li and Chen [28], using the Lattice-Boltzmann method. The optimal value for the above geometric parameters were found to be 0.6 for the groove width fraction (a measure of the groove asymmetry) and 5–6 grooves per half cycle.

Kang and Kwon [29] compared the flow characteristics in slanted groove, staggered herringbone and barrier embedded slanted groove micromixers using a coloured particle tracking method. Transverse velocity vector plots at different downstream locations as well as Poincaré maps obtained for all three micromixers indicated chaotic flow for both staggered herringbone and barrier embedded micromixers, but no notable chaotic mechanism was observed for slanted groove micromixers, in agreement with results reported earlier [21]. Particle tracers were labelled with a specific colour and the particle trajectories tracked for 20 periodic units. The coloured particle distributions were then used to evaluate the mixing quality both qualitatively as well as quantitatively, using a new method based on mixing entropy. The staggered herringbone was found to give the best mixing performance.

Liu et al. [30] presented a numerical study of mixing pure water and a solution of glycerol in water, in both the 3-D serpentine and staggered herringbone mixers. The effect of different fluid physical properties was examined by varying the amount of glycerol in the glycerol/water solution φ (i.e. the mass fraction of glycerol in water) at two different Reynolds number, $Re = 1$ and 10. The mixing performance at both Re, measured via a mixing index, decreased with increasing φ, although the variation in mixing index was smaller at higher Re. Tracer particles initially located at the two-fluid interface were advected inside the mixer and the distribution of tracer particles at the outlet cross-section were more or less identical at different Re and at different φ. Inspection of the cross-section mixing concentration profiles obtained from the numerical simulation revealed that the breakdown and deformation of the interface between the two fluids at $Re = 1$ and 10 were similar and independent of φ, although the gray intensity (which represents the mixedness of the two fluids) at lower Re (at all φ) was more uniform than the corresponding picture at higher Re. This was due to the longer residence time available for diffusional mixing at lower Re. The gray intensity gradually turned less uniform with increasing φ, at both Re, due to lower diffusivity values. Unlike the 3D serpentine mixers, the flow advection in the staggered herringbone mixer was not enhanced with increasing Re, in agreement with experimental observation [17].

The velocity generated by the grooves in a staggered herringbone mixer and the effect of varying Re on the generation of cross-channel flow and mixing have been investigated in detail by Hassell and Zimmerman [31]. Three representative geometries were evaluated; a single herringbone groove, a channel section representing one continuous herringbone cycle and a third representing a system in which the orientation of the grooves were constantly switched. As Re increased, the amount of entrained fluid in the groove decreases and the fluids in the groove move further across the groove before re-entering the bulk channel flow at the channel edges. Increasing the groove depth results in increased fluid entrainment in the grooves leading to an increase in transverse velocity component in the bulk flow, in agreement with earlier studies [25]. Successive grooves resulted in an increase in the transverse velocity components and a 14% increase in fluid entrainment in grooves compared to the case of the single groove. The fluid flow in the bulk channel flow was found to exhibit low helicity which increased slightly at higher Re.

Recently an alternative method for characterizing and quantifying the degree of mixing was presented by Camesasca et al. [32]. The Shannon entropy S, which has been previously employed for a variety of practical applications in polymer processing, was used to compare the mixing performance in a plain microchannel, a slanted groove microchannel as well as the staggered herringbone micromixer. The staggered herringbone mixer was shown to perform better than the slanted groove mixer, with no mixing observed in the plain channel, as expected. The method can also be applied to experimen-

tal data; using experimentally derived pictures of the mixer cross-section for the staggered herringbone mixer, the change in entropy with increasing number of cycles was compared to the values obtained numerically, with excellent agreement in both values. An alternative way to pattern ridges on the walls of a simple straight channel to achieve chaotic mixing was also presented [33]. Three types of non-periodic patterns were generated using the Weierstrass fractal function to position the tip of 'V' grooves on the bottom channel wall and the performance of these mixers was compared to a design which was similar to the staggered herringbone mixer. Qualitative analysis of the cross-sectional velocity field along the length of the channel as well as pathlines of particle trajectories and trajectory 'beams' confirmed the presence of chaotic flow for all four mixers. Evaluation of Lyapunov exponents allowed for a limited assessment of mixing behaviour while entropic analysis allowed a more global characterization of mixing performance. Two of the new mixers designed were found to be more efficient than the one based on the staggered herringbone mixer. Generalized fractal dimensions associated with the interface of the two fluids to be mixed were computed for all four mixer designs and the results were consistent with results from entropic mixing analysis.

In the current work, the flow behaviour of the staggered herringbone mixer is studied using computational fluid dynamics and particle tracking methods. Several methods which have previously been reported for characterising the mixing performance in macro-scale static mixers such as the coefficient of variance of the distribution of particle tracers and the stretching histories of the particles, are used. However, in contrast with previous work (where mixing quality is determined at a given position along the length of the mixer), a method for estimating the required mixing length for complete mixing, especially useful in designing micromixers, is described. Using the geometric mean stretch computed from the stretching histories, the minimum mixing length required for complete mixing is computed by taking into account the rate of striation reduction and diffusional penetration distance.

2. Numerical methods

The mixer geometry used was kept consistent with that reported by Stroock et al. [17]. The channel width is 200 μm and the channel height is 85 μm. The staggered herringbone mixer is composed of several mixing cycles in series. Each mixing cycle is composed of two sets of herringbone grooves which are asymmetric with respect to the centre of the channel in the axial direction. The orientation of the asymmetric herringbones is switched between each half cycle, allowing a corresponding switch in the centre of rotation in the transverse flow. The grooves are placed at an angle θ with respect to the axial direction and the degree of asymmetry p is measured by the fraction of channel width occupied by the wide arm of the herringbones.

The full depth of the grooves is 30.6 μm, given by $2ah$, where a is the ratio of groove half-depth to full channel height and the groove wave vector, $\boldsymbol{q}$ is $2\pi/100\ \mu m^{-1}$, as shown in Fig. 1. Due to the repeating cycles, the velocity field in the axial direction can be assumed to be periodic and hence the velocity field in one mixing cycle can be obtained and reused repeatedly for successive cycles. Details of the mixer geometry and fluid properties are summarised in Table 1.

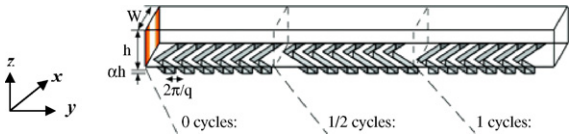

Fig. 1. Staggered herringbone mixer (from [17]).

2.1. Velocity field

The 3D velocity field for one complete mixing cycle was computed using COMSOL Multiphysics which is a commercial modelling software based on the finite element method. The simulations were run as steady state incompressible Navier–Stokes flow, with periodic boundary conditions at both inlet and outlet. This enables long streamline integrations to be performed using the velocity field of a single mixing cycle if entrance flow effects are neglected. No-slip boundary conditions were applied at all other channel walls. The volumetric flow through the mixer was set by specifying a pressure drop and setting the pressure at the outlet equal to the pressure at the inlet minus the pressure drop. The number of mesh elements in the model is 30712 and the simulations were performed on Windows XP with Pentium IV 3.00 GHz CPU and 2 GB of RAM.

Evaluation of mixing performance is typically carried out by simultaneously solving the Navier–Stokes and continuity equations for the velocity field and the convection–diffusion equations for the concentration profiles in the mixer. However, this approach introduces artificial diffusive fluxes due to discretisation errors, especially for liquid/liquid mixing [10,22]. Lagrangian particle tracking methods, where the trajectories of massless tracer particles are computed have been used to characterize the mixing performance, to avoid numerical diffusion problems [18–21,24,25,29]. The 3D velocity field was first computed as described above. Streamline integration of the velocity field described in the following section, allows the particle trajectories in the micromixer to be computed.

Table 1
Mixer geometry and fluid properties

Mixer	
Channel width, w (μm)	200
Channel depth, h (μm)	85
Length per cycle (mm)	1.516
Number of grooves per cycle	12
Relative groove depth (a)	0.18
Wave vector, $\boldsymbol{q}$ (μm^{-1})	$2\pi/100$
Groove asymmetry, p	2/3
Groove angle, θ (°)	45
Fluid properties	
Density (kg/m^3)	1200
Viscosity (Pa s)	0.067

2.2. Particle tracking computations

The particle trajectories in the herringbone mixer were obtained by solving the vector equation of motion for each particle:

$$\frac{d\boldsymbol{x}}{dt} = \boldsymbol{v}(\boldsymbol{x}) \quad (1)$$

For a particle at a given location (x, y, z), the particle velocity is obtained by interpolating the velocity field from the solution of the Navier–Stokes and continuity equations. The COMSOL particle tracking algorithm was modified to allow for the velocity field obtained in a single mixing cycle to be utilised over successive mixing cycles. The algorithm to achieve this was set up as follows:

(i) Based on the particle axial position and mixer length per cycle, establish in which cycle number the particle is located.
(ii) Determine the equivalent position in the first mixing cycle (where the velocity field solution is available).
(iii) Interpolate the velocity field solution to obtain the velocity at that position.
(iv) Calculate new position by solving (1).

The particle moves to a new position down the channel length at every time step, information about the new coordinates is stored and the procedure repeated for the specified number of time steps. A standard fourth order Runge-Kutta method with fixed time steps was used. The size of the time step was selected carefully to avoid losing particles (too big a time step will result in the particle moving to a position outside the solution domain and the particle is then 'lost') while at the same time avoiding excessive computation time. The simulations were carried out at two time different steps, at h and $h/2$, and the results compared. If the difference between the two was small, then the solution at h was accepted, otherwise the time step was reduced and the procedure repeated. The coordinates of the particle at the end of every mixing cycle were recorded.

2.3. Stretching

The stretching of material lines and surfaces by a flow is useful for determining the interfacial area between components which is a measure of the mixed state. A convenient means of characterizing the stretching by the flow is to study the local behaviour of small material vectors. A second particle tracking algorithm was set up which allows the stretching of an infinitesimal material vector $\boldsymbol{l}$ associated with each tracer particle to be computed in addition to tracking the position of particles [18,19], using a fourth order Runge-Kutta method with adaptive time stepping. At the start of the mixer, the initial position of each tracer particle was specified and an initial material vector, $\boldsymbol{l}_{t=0} = [1, 0, 0]$ was assigned to each tracer particle. The evolution of vector $\boldsymbol{l}$ is tracked by integrating (1) together with

$$\frac{d\boldsymbol{l}}{dt} = (\nabla \boldsymbol{v})^T \boldsymbol{l} \quad (2)$$

The total accumulated stretching λ experienced by each element after some time is defined as

$$\lambda = \frac{|\boldsymbol{l}|}{|\boldsymbol{l_0}|} \quad (3)$$

3. Results and discussion

3.1. Flow patterns

The cross-sectional velocity vector plots at various locations along one mixing cycle at $Re = 0.01$, as indicated in Fig. 2(a), are shown in Fig. 2(b). The flow patterns are complex with a strong transverse component (x and z components). As the flow moves along in the axial direction, two counter rotating vortices are produced, one large and one small, which meet over the sharp edge (at $x = 1.3$ for locations A and B and $x = 0.7$ for locations C and D) of the herringbone grooves (see Fig. 2) and alternate periodically depending on the direction of asymmetry of the herringbone grooves. The maximum and minimum velocity in the x, y and z directions are also indicated in Fig. 2, where the negative sign represents flow in the opposite direction. The velocity vector plots are in agreement with those reported elsewhere [24,29]. The transverse flow velocity is approximately an order of magnitude lower than the forward axial component, with the velocity in the long arm of the herringbone higher than that in the short arm. Fig. 3 shows the trajectories for 10 particles initially located across the mixer cross-section. The particle trajectories show small-scale helical motion similar to the results of Wang et al. [21], which indicates folding and stretching of fluids. The herringbone grooves aid mixing not only by creating secondary helical flow but also by 'ditch mixing' where fluid from one side of the channel is transported to the opposite side of the channel in the grooves and rolls out from the grooves at the side edge back into the main flow in the channel [34]. This results in increased contact area between the two fluids that enhance mixing. Mixing in the staggered herringbone mixer is therefore enhanced by both the strong transverse flow which stretches and folds the fluid interface and increased contact area by ditch mixing.

3.2. Mixing simulation

To visualize the mixing in the staggered herringbone mixer, ~8000 tracer particles were initially placed uniformly in one-half of the channel cross-section at the mixer entrance, starting at 5 μm away from the walls in the x-direction and 2 μm away from the z-direction, corresponding to around 2% of the length scales in both directions, to avoid particles getting trapped in those areas where the velocity is close to zero. All tracer particles were released simultaneously and the position of the tracer particles was tracked along the mixer length as described earlier. The tracer particles travel along the mixer length at different speeds due to the laminar flow profile and the presence of dead volumes

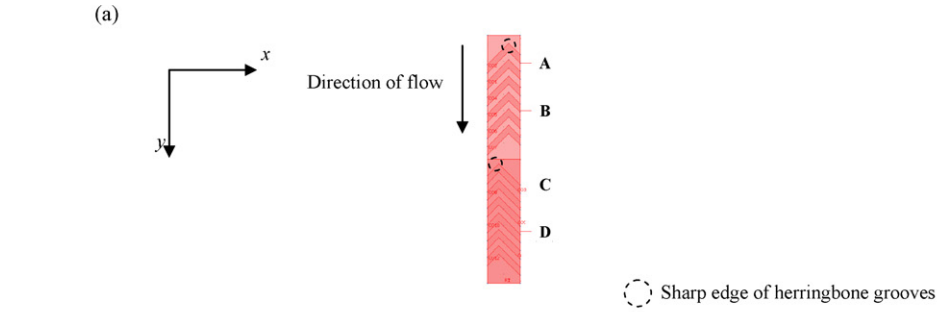

(b)

Section A

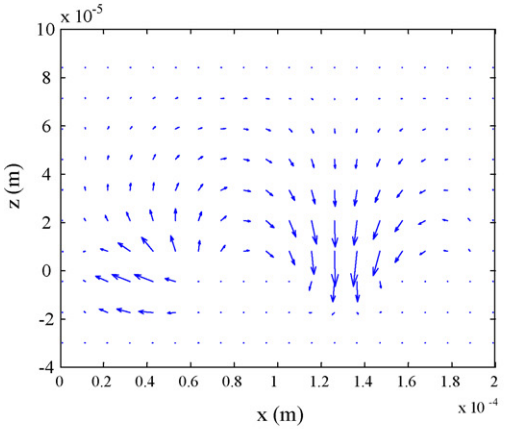

Velocity (m/s)	Max	Min
V_x	1.4 x 10^{-4}	-3.0 x 10^{-4}
V_y	3.8 x 10^{-3}	-8.8 x 10^{-6}
V_z	2.3 x 10^{-4}	-5.2 x 10^{-4}

Section C

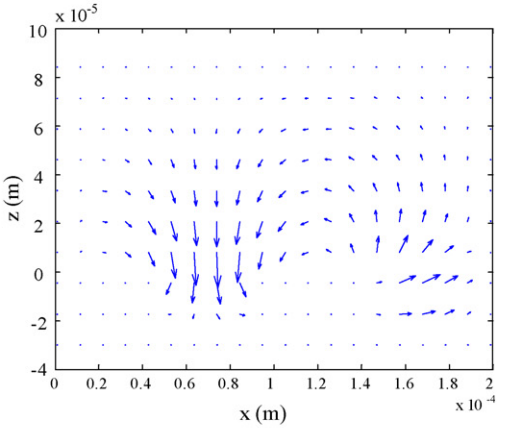

Velocity (m/s)	Max	Min
V_x	2.8 x 10^{-4}	-1.1 x 10^{-4}
V_y	3.8 x 10^{-3}	-9.6 x 10^{-6}
V_z	2.4 x 10^{-4}	-4.9 x 10^{-4}

Section B

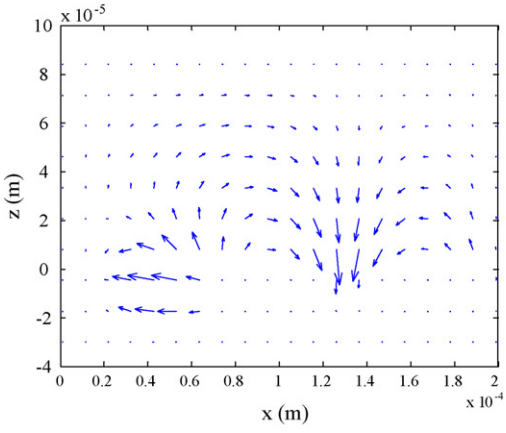

Velocity (m/s)	Max	Min
V_x	1.3 x 10^{-4}	-3.6 x 10^{-4}
V_y	3.8 x 10^{-3}	-2.3 x 10^{-5}
V_z	2.1 x 10^{-4}	-4.3 x 10^{-4}

Section D

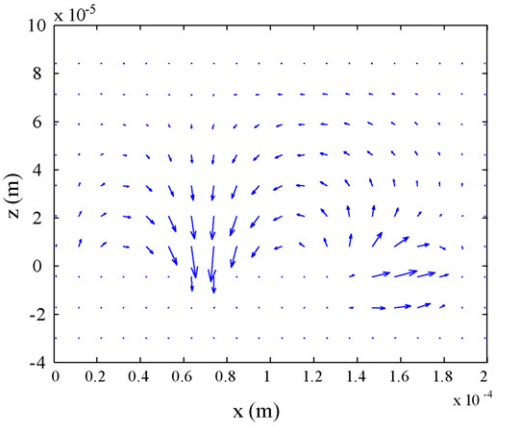

Velocity (m/s)	Max	Min
V_x	3.4 x 10^{-4}	-1.4 x 10^{-4}
V_y	3.8 x 10^{-3}	-1.1 x 10^{-5}
V_z	2.1 x 10^{-4}	-5.0 x 10^{-4}

Fig. 2. Cross-sectional velocity vector plots at various axial positions for $Re = 0.01$. (a) Axial position of the cross-sectional velocity vector plots. (b) Velocity vector plots.

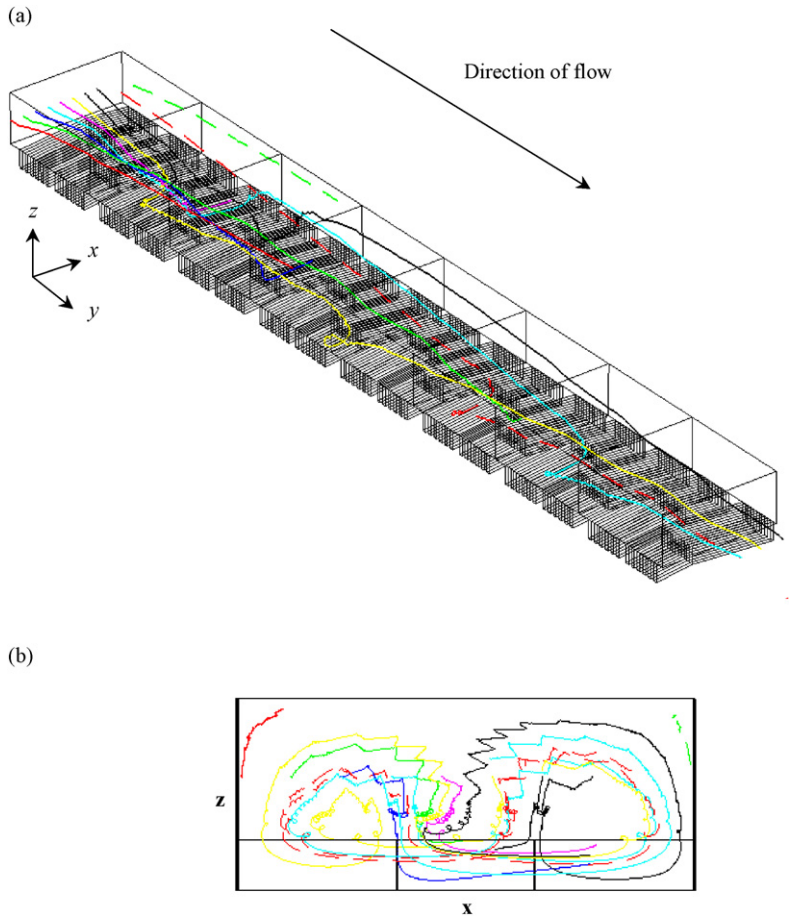

Fig. 3. Particle trajectories at 10 different initial locations ([x (μm), z (μm)] = [1, 38], [23, 38], [45, 38], [67, 38], [89, 38], [111, 38], [133, 38], [155, 38], [177, 38], [199, 38]) along eight mixing cycles for t = 0–10 s and Re = 0.01. (a) 3D view (y direction is compressed). (b) X–Z plane viewed from outlet.

in the herringbone grooves. Plots of particle distribution in the mixer cross-section were obtained by recording the particle positions once they reached the end of each mixing cycle. This yields striation patterns which are equivalent to those observed with a continuous feed at steady state with the same initial conditions because the trajectories followed by the tracer particles are time independent; a tracer follows the same path as all other tracers that pass through the same starting position regardless of its time of introduction [26]. The mixing simulations were carried out at Re = 0.001, 0.01, 0.03, 1 and 10. The first three conditions (Re = 0.001, 0.01 and 0.03) correspond to three experimental conditions used by Stroock et al. [17]. The last two conditions were selected so that the effect of a larger range of Reynolds number can be evaluated.

The mixer cross-sectional plots at $Re \sim 0.01$ at the mixer inlet and at various locations downstream of the entrance are shown in Fig. 4. The simulation plots were compared to published experimental confocal micrographs at the same conditions [17] and the evolution of striation patterns can be seen to be qualitatively similar, indicating that the numerical simulation method used can capture the flow phenomena accurately. Small differences between the simulation and experimental micrographs can be attributed to the fact that the computed velocity field assumes identical fluid properties for the two inlets to be mixed as this allows the velocity field to be used repeatedly over successive mixing cycles while in practice this was clearly not the case. Additionally, the simulation plots do not take into account molecular diffusion effects. The simulation plots were also observed to be qualitatively similar to simulation plots reported elsewhere [26,29]. The cross-sectional plots at the same axial positions were observed to be qualitatively similar at all Re, with no major differences in the patterns of the tracer particles. The flow advection in a staggered herringbone mixer was found to be independent of Reynolds number, in agreement with other numerical studies on the staggered herringbone mixer [26,30] as well as experimental results where the flow patterns were found to be qualitatively similar up to Re = 100 [17].

3.3. Coefficient of variance

While the mixing simulations allowed for a qualitative assessment of mixing in a staggered herringbone mixer, a quantitative description of the mixing quality affords a more practical means of evaluating the mixing performance. The tracer mixing simulations, carried out with N_{T0}, the total number of particles = 7872 and evaluated at Re = 0.001, 0.01, 0.03, 1 and 10 were quantified by computing the number-based coefficient of variance (also known as relative standard deviation), which is the standard deviation of the particle distribution divided by the mean. An x–z grid of 20 × 10 equal-sized cells (each cell with approxi-

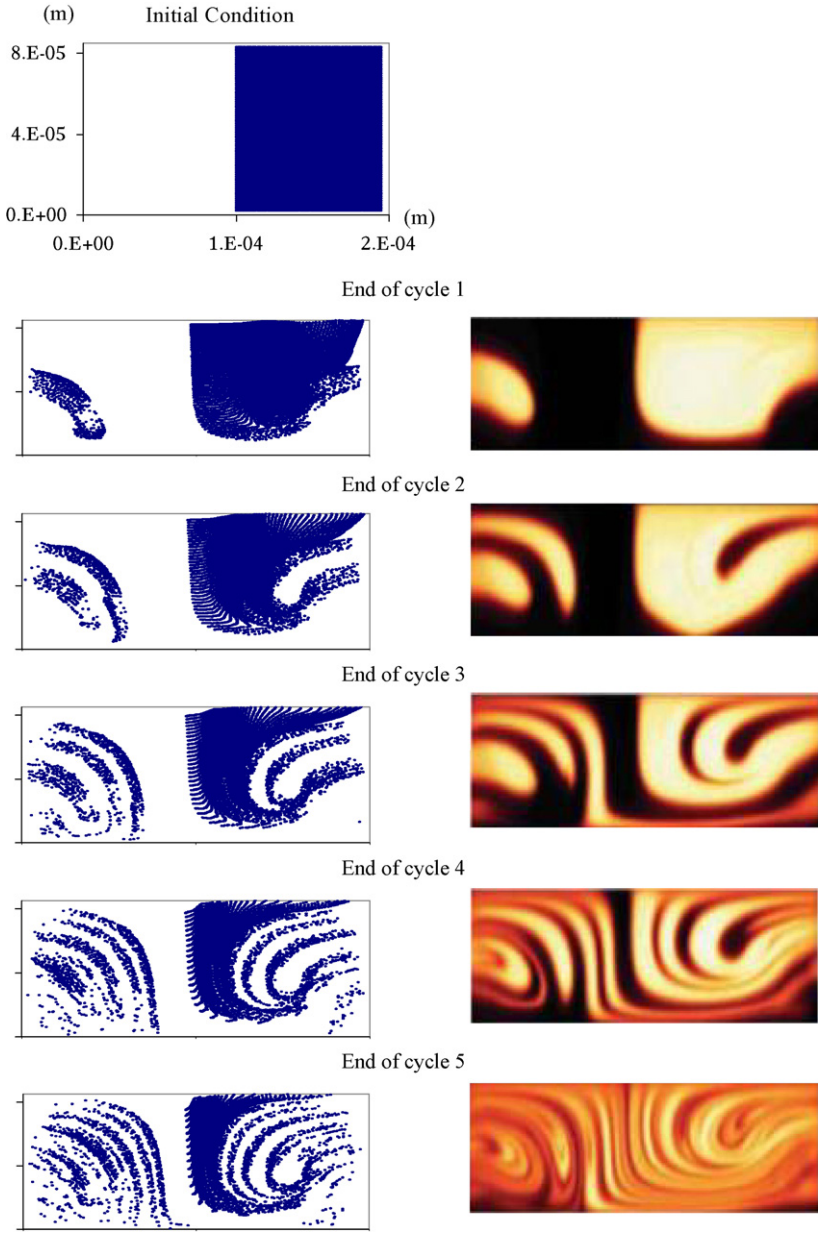

Fig. 4. Comparison of the evolution of particle tracer positions along the mixer length with confocal micrographs (from [17]) of an actual staggered herringbone mixer. Both the simulation plot and experimental confocal micrographs were obtained at $Re = 0.01$.

mate dimensions of 10 μm × 8.5 μm) was placed over the mixer cross-section at the end of each mixing cycle. The number of particles in each cell, N_i was computed based on the position of each particle on the mixer cross-section and the average particle concentration per cell was then computed as $\bar{N} = N_T/(20 \times 10)$, where N_T is the total number of particles within the grid at the end of each mixing cycle. The variance σ^2 was calculated from

$$\sigma^2 = \frac{\sum_{i=1}^{M}(N_i - \bar{N})^2}{M-1}, \quad M = 20 \times 10 \tag{4}$$

The number based coefficient of variance (COV) was then computed from the following equation:

$$\mathrm{COV} = \frac{\sigma}{\bar{N}} \tag{5}$$

When the COV is zero, an ideal homogenization of the mixture is obtained. The coefficient of variance at different mixing cycles can be fitted to an equation of the form

$$\frac{\sigma}{\bar{N}} = A\exp(-Bn), \quad n = \text{mixing cycle number} \tag{6}$$

The coefficient B [18,19] represents the rate of decrease of the coefficient of variance per mixing cycle and provides a simple quantitative estimate of the mixing rate while the coefficient A represents the coefficient of variance of the unmixed inlet stream. The results of the coefficient of variance plotted against the number of mixing cycles at different Reynolds number is shown in Fig. 5. The calculated coefficient of variance gradually decreases with increasing number of cycles at all values of Re. The change in coefficient of variance with increasing number

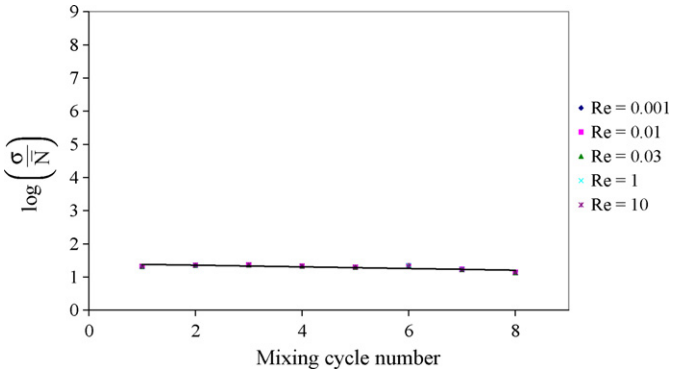

Fig. 5. Change in coefficient of variance with number of mixing cycles at various *Re* (All data points at different *Re* overlap).

of cycles at $Re = 0.001$ to 10 were observed to be very similar. The value of the coefficient B was $\sim 0.023 \pm 0.002$ in all cases considered, indicating little difference in mixing rates. This is consistent with the qualitative evaluation of the striation patterns formed, which were observed to be independent of *Re*.

The total number of particles at each end-of-cycle cross-section gradually decreases from the initial number of particles released at the inlet, resulting in decreasing number of tracked points with increasing mixer cycle, which affects the accuracy of the calculations. This is due to increasingly more particles being left behind in the cycle grooves, as a result of the dead volumes in the mixer. The number of tracked points reduced by an average of 201 particles for every cycle, which represents an average reduction of 6% per cycle. Additionally, the grid size used in the calculations may limit the resolution of mixture homogenization. While increased resolution can be obtained by using a finer grid, this would also require a much larger number of particles to be tracked (to minimise statistical uncertainty), hence the number of grid cells cannot be increased indefinitely (see [18]). In this sense, the coefficient of variance and other statistical methods of quantifying mixers are probably not a good method for comparing mixing performance in the staggered herringbone mixer.

3.4. Stretching

Another method which has been used to quantify the rate of mixing is the computation of the stretching histories along with the trajectories of a set of material elements placed within the flow [18,19,24]. This method has been employed in evaluating the mixing and chaotic behaviour in two-dimensional, time periodic flows as well as three-dimensional static mixers. The key to effective mixing is in producing the maximum amount of interfacial area between two initially segregated fluids in the minimum amount of time. The amount of intermaterial surface generated in a region is directly proportional to the amount of stretching experienced by fluid elements in that region; regions with high rates of stretching provide good mixing while regions with low rates of stretching provide poor mixing. The distance between striations, is inversely proportional to the surface area. Hence, the rate of stretching and folding affects the rate of micromixing by both reducing the striation thickness (and hence the diffusional distance) and increasing the interfacial area for interdiffusion of components [35]. Chaotic flow is associated with an exponential increase in stretching and folding, resulting in a corresponding decrease in the axial length required for complete mixing. Stretching computations can be used to evaluate the chaotic behaviour and hence mixing efficiency in the mixers, which for a time periodic system, can be expressed by the Lyapunov exponent, $\delta = \lim_{t\to\infty} (\ln \lambda / t)$ [24,36]. The stretching computations can also be used to characterize the distribution of mixing intensities from the distribution of stretching magnitudes in the mixer flow [18,19].

For the stretching calculations, 4100 particles were placed uniformly across the channel cross-section at the mixer entrance, 5 μm away from the channel walls in the x-direction and 2 μm away in the z-direction. The tracer particle position and the accumulated length stretch were tracked along the mixer length as described earlier. At every periodic plane, both the tracer particle position and the components of the stretch vector were recorded. The geometric mean stretching values for all N tracer particles was computed at every periodic plane from

$$\lambda_{g,50} = \left(\prod_{i=1}^{N} \lambda_i \right)^{1/N} \tag{7}$$

The specific stretch per period, α_{50} for a spatially periodic flow, which is the direct analog of the Lyapunov exponent, δ for a time periodic flow [18,19,24], was computed from

$$\alpha_{50} = \lim_{n\to\infty} \left[\frac{1}{n} \ln \lambda_{g,50} \right], \quad n = \text{mixing cycle number} \tag{8}$$

The $\ln \langle \lambda_{g,50} \rangle$ is plotted against the number of mixing cycles in Fig. 6 for $Re = 0.001$, 0.01, 0.03, 1 and 10. In chaotic flows, the value α_{50} tends to positive limit values implying exponential stretching and growth of inter material area (on average) while in regular flows this value tends to zero [36]. The values of α_{50} at different Reynolds number were obtained from the gradients of the plots in Fig. 6. The mean stretch, $\lambda_{g,50}$ increases exponentially with the number of mixing cycles at every Reynolds number considered. The values of α_{50} were found to be similar with no particular trend with respect to *Re* with $\alpha_{50} = 0.75 \pm 0.01$ in all cases. From the results of the mixing simulations, the form

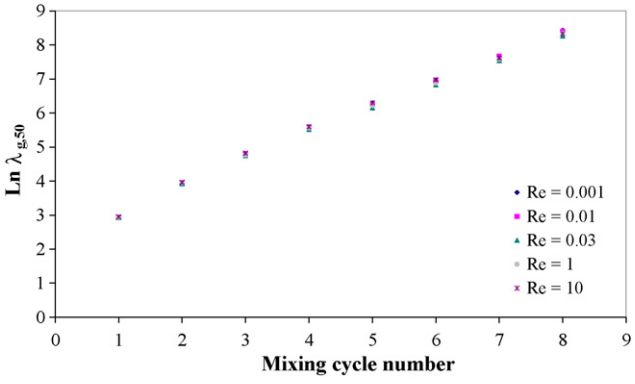

Fig. 6. Change in mean stretch of all vectors, $\lambda_{g,50}$ vs. number of mixing cycles at various *Re* (data points at different *Re* overlap).

of the flow remains qualitatively the same at different *Re* number, which is in agreement with published findings [17,26,30]. The difference in mixing uniformity at various *Pe* number observed experimentally can be attributed to the effects of molecular diffusion and hence to compute the required length for complete mixing, the role of molecular diffusion must also be considered.

3.5. Mixing length calculation

As mentioned earlier, the exponential stretching of fluid elements accelerates mixing in two different ways, that is by reducing the striation thickness and by generating a greater interfacial area for molecular diffusion. The ratio of penetration distance by molecular diffusion to striation thickness for a time-periodic system evolves along the mixer length according to [35]

$$\frac{\delta_x}{s(0)\,\mathrm{e}^{-\delta t}} = \left[\frac{D}{(s(0))^2 2\delta}(e^{2\delta t} - 1)\right]^{1/2} \tag{9}$$

For a spatially periodic flow, the penetration distance due to molecular diffusion increases along the mixer length while the striation thickness is reduced from $s(0)$ to $s(n)$, according to the stretching function, α. Eq. (9) for a spatially periodic system then becomes

$$\frac{\delta_x}{s(0)\,\mathrm{e}^{-\alpha n}} = \left[\frac{D\tau}{(s(0))^2 2\alpha}(\mathrm{e}^{2\alpha n} - 1)\right]^{1/2} \tag{10}$$

where τ is the residence time per mixing cycle. Mixing is assumed to be complete when the penetration distance from molecular diffusion becomes equal to the striation thickness [35]. This happens when

$$1 = \left[\frac{D\tau}{(s(0))^2 2\alpha}(\mathrm{e}^{2\alpha n} - 1)\right]^{1/2} \tag{11}$$

Rearranging Eq. (11), n_{mix} the number of mixing cycles required (and hence y, the length) for complete mixing is determined from

$$n_{\mathrm{mix}} = \frac{\ln(((s(0))^2 2\alpha/D\tau) + 1)}{2\alpha} \tag{12}$$

$$y = n_{\mathrm{mix}} \cdot L_{\mathrm{cycle}} \tag{13}$$

The required mixing lengths (y_{50}) computed using the mean stretch values (α_{50}) are shown in Fig. 7 along with mixing lengths obtained experimentally by Stroock et al. [17]. The mixing lengths calculated using the specific stretch per period were observed to be different from those derived experimentally.

This can be due to the following:

- The experimentally derived values are based on measurements in the central 50% of the cross-sectional area, where striation thickness reduction is much slower than say, at the bottom or sides of the channel. Additionally, the experimentally derived mixing lengths were determined for 90% mixing.
- The specific stretch per period used to compute the mixing lengths was derived from the mean stretch values in each period (this represents rate of increase in the mean stretch values with increasing mixing cycle), when in reality there exists a log-normal distribution of stretch values [35], as shown in Fig. 8. The scatter plots represent the probability density calculated from frequency data for the stretch values at various mixing cycles while the smooth lines represent normal distribution curves fitted using the computed mean and standard deviation values. The normal distribution is defined as the distribution with density:

$$f(X) = \frac{1}{\sigma\sqrt{2\pi}}\,\mathrm{e}^{-1/2(X-m/\sigma)^2} \tag{14}$$

where X represents $\ln(\lambda)$, m represents the mean and σ represents the standard deviation.
- The accuracy of the computed stretch values can be sensitive to the time step used. While this problem may be alleviated using a smaller time step and implementing adaptive time-step control, there is a trade-off between using an infinitely small time step to improve accuracy and running the simulation for a sufficiently long time to ensure a substantial number of particles are advected to the end of the mixing cycles (smaller time step means that for the same run time, the particles may not reach the same axial distance downstream of the entrance, resulting in smaller sample size).

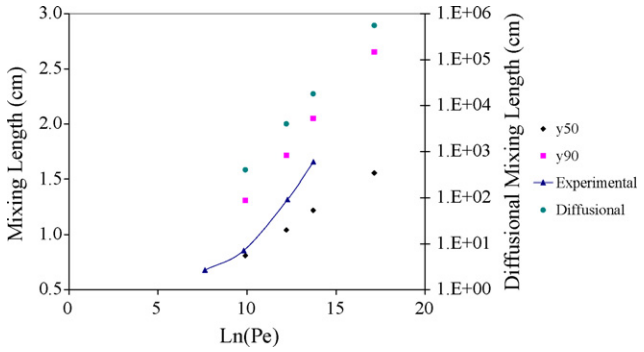

Fig. 7. Computed and experimentally derived mixing lengths vs. ln(*Pe*).

In the design of mixers, it is of interest to ensure that the mixer length provided can achieve sufficient mixing. One way of doing this, which avoids the problems mentioned above, is by using a method which allows a conservative estimate of required mixing length to be made. This can be done by replacing the geometric mean stretching $\lambda_{g,50}$, which represents the cut-off point at which 50% of the stretch values have a higher value, with a lower cut-off point in which at least 90% of the stretch values are higher. Using the z-score,[1] this lower cut-off point was determined to be at 1.2816 times the standard deviation below the mean, as illustrated in Fig. 9(inset). The logarithm of $\langle\lambda_{g,90}\rangle$ is plotted against the number of mixing cycles in Fig. 9. The values of α_{90} (which represents the rate of increase of $\lambda_{g,90}$) at

[1] The z-score for a value y of a data set is the distance that y lies above or below the mean, measured in units of the standard deviation. The z-score is defined as $z = y - m/\sigma$. The cut-off point was determined from a table of normal curve areas [37].

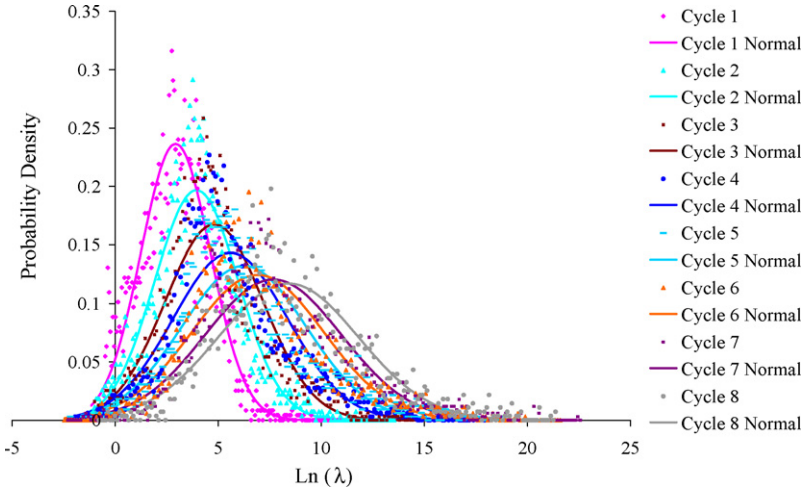

Fig. 8. Log-normal distribution of stretch values at $Re = 0.01$.

different Reynolds number were calculated from the gradients of the plots in Fig. 9, to be $=0.43 \pm 0.01$ for all cases. This gives a conservative mixing length value and can be thought of as the point where 90% of the mixture has a penetration distance at least equal to the striation thickness. The required number of mixing cycles and hence mixing length can be similarly obtained from equations:

$$n_{90} = \frac{\ln(((s(0))^2 2\alpha_{90}/D\tau) + 1)}{2\alpha_{90}} \quad (15)$$

$$y_{90} = n_{90} \cdot L_{\text{cycle}} \quad (16)$$

As seen in Fig. 7, the staggered herringbone mixer allows rapid mixing even at high *Pe* numbers. In the same figure, the required mixing length in a plain channel with characteristic length *d*, by diffusion alone is plotted from $y_{\text{dif}} = \bar{u}\, x(d^2/D) = d\ x\ Pe$ (see "Diffusional" in Fig. 7). It is clearly seen that the herringbone mixer shows a marked reduction in mixing length to that required for diffusive mixing alone.

3.6. Pressure drop

The pressure drop across one cycle of the staggered herringbone mixer was obtained from the velocity field simulation and is presented in Fig. 10 as a function of *Re*. For comparison, the pressure drop across a grooveless channel of the same dimensions is also plotted in Fig. 10. The latter is calculated using

$$\Delta P = \frac{128\mu L Q}{\pi d_{\text{E}}^4} \quad (17)$$

The pressure drop increased linearly with Reynolds number and was slightly lower than the pressure drop in a grooveless channel by 7.5% at $Re < 10$. It has been previously reported that the presence of grooves effectively weakens the no-slip condition, resulting in lowering of the pressure drop compared to that in a simple grooveless channel [34]. The groove type, groove depth and number of grooves per cycle have negligible effect on the pressure drop although the width of the grooves appears to have a stronger effect on pressure drop [24,25]. These results further demonstrate the potential benefits of using the staggered herringbone mixer to enhance mixing, as unlike static mixing elements, the presence of the grooves reduce the energy costs compared to a plain channel.

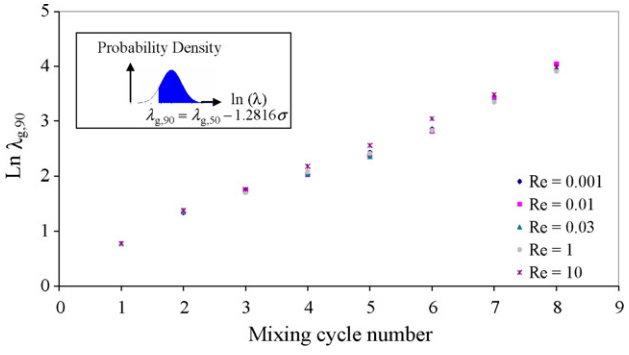

Fig. 9. Change in stretch value, $\lambda_{g,90}$ vs. number of mixing cycles at various *Re* (data points at different *Re* overlap).

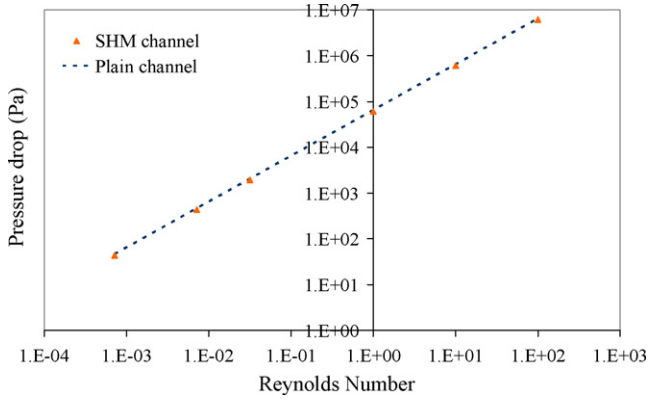

Fig. 10. Change in pressure drop across one mixing cycle with Reynolds number.

4. Conclusions

The mixing performance of the staggered herringbone mixer was evaluated numerically at $Re = 0.001–10$. The velocity field was obtained via CFD simulations. Particle tracking methods were used to quantify the mixing performance to avoid numerical diffusion problems. Mixing is enhanced in the staggered herringbone mixer by the formation of a double helical flow in the mixer which alternates from one side of the channel to the other, depending on the asymmetry of the herringbone grooves as well as by ditch mixing, where fluid from one side of the channel is transported to the opposite side via the grooves, resulting in increased contact area for mixing. The particle distribution at the end of every mixing cycle was obtained for all cases and the striation patterns were found to be qualitatively similar to published work.

Several methods to quantify the mixing performance of the staggered herringbone mixer were investigated. The coefficient of variance at the end of each mixing cycle was computed and the mixing quality was found to be independent of *Re*. The stretching histories for material elements associated with each particle tracer were also computed. The specific stretch per cycle was obtained from the stretching calculations and taking into account the effects of diffusion, the mixing length required for complete mixing was evaluated. The calculated mixing lengths were lower than experimentally derived values. The difference in calculated and experimentally derived values could be due to the fact that the experimentally derived values were based on measurements in the central 50% of the mixer cross-sectional area. Additionally, the specific stretch per cycle used to compute the mixing lengths were derived from the mean stretch values in each cycle, while in practice, there exists a log-normal distribution of stretch values. Using $\alpha_{90,}$ which represents the rate of increase of $\lambda_{g,90}$ values (cut-off point for λ_g in which 90% of the computed stretch values are higher), allowed for a conservative estimate of required mixing length to be made.

Acknowledgement

Financial support by the DTI/EPSRC Foresight LINK programme is gratefully acknowledged.

References

[1] D. Gobby, P. Angeli, A. Gavriilidis, Mixing characteristics of T-type microfluidic mixers, J. Micromech. Microeng. 11 (2) (2001) 126–132.
[2] S.H. Wong, M.C.L. Ward, C.W. Wharton, Micro T-mixer as a rapid mixing micromixer, Sens. Actuators B: Chem. 100 (3) (2004) 359–379.
[3] S. Hardt, F. Schönfeld, Laminar mixing in different interdigital micromixers. II. Numerical simulations, AICHE J. 49 (3) (2003) 578–584.
[4] V. Hessel, S. Hardt, H. Löwe, F. Schönfeld, Laminar mixing in different interdigital micromixers. I. Experimental characterization, AICHE J. 49 (3) (2003) 566–577.
[5] P. Löb, K.S. Drese, V. Hessel, S. Hardt, C. Hofmann, H. Löwe, R. Schenk, F. Schönfeld, B. Werner, Steering of liquid mixing speed in interdigital micro mixers—from very fast to deliberately slow mixing, Chem. Eng. Technol. 27 (3) (2004) 340–345.
[6] F. Schönfeld, V. Hessel, C. Hofmann, An optimised split-and-recombine micro-mixer with uniform 'chaotic' mixing, Lab Chip 4 (1) (2004) 65–69.
[7] K.S. Drese, Optimization of interdigital micromixers via analytical modelling—exemplified with the SuperFocus mixer, Chem. Eng. J. 101 (1–3) (2004) 403–407.
[8] V. Mengeaud, J. Josserand, H.H. Girault, Mixing processes in a zigzag microchannel: Finite element simulations and optical study, Anal. Chem. 74 (16) (2002) 4279–4286.
[9] C.P. Jen, C.Y. Wu, Y.C. Lin, C.Y. Wu, Design and simulation of the micromixer with chaotic advection in twisted microchannels, Lab Chip 3 (2) (2003) 77–81.
[10] F. Jiang, K.S. Drese, S. Hardt, M. Kupper, F. Schönfeld, Helical flows and chaotic mixing in curved micro channels, AICHE J. 50 (9) (2004) 2297–2305.
[11] R.H. Liu, M.A. Stremler, K.V. Sharp, M.G. Olsen, J.G. Santiago, R.J. Adrian, H. Aref, D.J. Beebe, Passive mixing in a three-dimensional serpentine microchannel, J. Microelectromech. Syst. 9 (2) (2000) 190–197.
[12] S. Hardt, K.S. Drese, V. Hessel, F. Schönfeld, Passive micromixers for applications in the microreactor and μTAS fields, Microfluid. Nanofluid. 1 (2) (2005) 108–118.
[13] V. Hessel, H. Löwe, Mixing Principles for Microstructured Mixers: Active and Passive Mixing. Microreactor Technology and Process Intensification, ACS Symposium Series, 2005.
[14] V. Hessel, H. Löwe, F. Schönfeld, Micromixers—a review on passive and active mixing principles, Chem. Eng. Sci. 60 (8–9) (2005) 2479–2501.
[15] N.T. Nguyen, Z.G. Wu, Micromixers—a review, J. Micromech. Microeng. 15 (2) (2005) R1–R16.
[16] T.J. Johnson, D. Ross, L.E. Locascio, Rapid microfluidic mixing, Anal. Chem. 74 (1) (2002) 45–51.
[17] A.D. Stroock, S.K.W. Dertinger, A. Ajdari, I. Mezic, H.A. Stone, G.M. Whitesides, Chaotic mixer for microchannels, Science 295 (2002) 647–651.
[18] D.M. Hobbs, F.J. Muzzio, The Kenics static mixer: a three-dimensional chaotic flow, Chem. Eng. J. 67 (3) (1997) 153–166.
[19] D.M. Hobbs, F.J. Muzzio, Reynolds number effects on laminar mixing in the Kenics static mixer, Chem. Eng. J. 70 (2) (1998) 93–104.
[20] D.M. Hobbs, P.D. Swanson, F.J. Muzzio, Numerical characterization of low Reynolds number flow in the Kenics static mixer, Chem. Eng. Sci. 53 (8) (1998) 1565–1584.
[21] H.Z. Wang, P. Iovenitti, E. Harvey, S. Masood, Numerical investigation of mixing in microchannels with patterned grooves, J. Micromech. Microeng. 13 (6) (2003) 801–808.
[22] F. Schönfeld, S. Hardt, Simulation of helical flows in microchannels, AICHE J. 50 (4) (2004) 771–778.
[23] A.D. Stroock, S.K. Dertinger, G.M. Whitesides, A. Ajdari, Patterning flows using grooved surfaces, Anal. Chem. 74 (20) (2002) 5306–5312.
[24] J. Aubin, D.F. Fletcher, J. Bertrand, C. Xuereb, Characterization of the mixing quality in micromixers, Chem. Eng. Technol. 26 (12) (2003) 1262–1270.
[25] J. Aubin, D.F. Fletcher, C. Xuereb, Design of micromixers using CFD modelling, Chem. Eng. Sci. 60 (8–9) (2005) 2503–2516.
[26] A.D. Stroock, G.J. McGraw, Investigation of the staggered Herringbone mixer with a simple analytical model, Philos. Trans. R. Soc. Lond. Ser. A: Math. Phys. Eng. Sci. 362 (1818) (2004) 971–986.
[27] J.T. Yang, K.J. Huang, Y.C. Lin, Geometric effects on fluid mixing in passive grooved micromixers, Lab Chip 5 (10) (2005) 1140–1147.
[28] C.A. Li, T.N. Chen, Simulation and optimization of chaotic micromixer using lattice Boltzmann method, Sens. Actuators B: Chem. 106 (2) (2005) 871–877.
[29] T.G. Kang, T.H. Kwon, Colored particle tracking method for mixing analysis of chaotic micromixers, J. Micromech. Microeng. 14 (7) (2004) 891–899.
[30] Y.Z. Liu, B.J. Kim, H.J. Sung, Two-fluid mixing in a microchannel, Int. J. Heat Fluid Flow 25 (6) (2004) 986–995.
[31] D.G. Hassell, W.B. Zimmerman, Investigation of the convective motion through a staggered Herringbone micromixer at low Reynolds number flow, Chem. Eng. Sci. 61 (9) (2006) 2977–2985.

[32] M. Camesasca, I. Manas-Zloczower, M. Kaufman, Entropic characterization of mixing in microchannels, J. Micromech. Microeng. 15 (11) (2005) 2038–2044.
[33] M. Camesasca, M. Kaufman, I. Manas-Zloczower, Staggered passive micromixers with fractal surface patterning, J. Micromech. Microeng. 16 (11) (2006) 2298–2311.
[34] J.P. Bennett, C.H. Wiggins, A computational study of mixing microchannel flows, in: American Physical Society, Annual APS March Meeting, March 3–7, 2003.
[35] J.M. Ottino, S. Wiggins, Introduction: mixing in microfluidics, Philos. Trans. R. Soc. Lond. Ser. A: Math. Phys. Eng. Sci. 362 (1818) (2004) 923–935.
[36] D.V. Khakhar, J.G. Franjione, J.M. Ottino, A case-study of chaotic mixing in deterministic flows—the partitioned-pipe mixer, Chem. Eng. Sci. 42 (12) (1987) 2909–2926.
[37] W. Mendenhall, T. Sincich, Statistics for Engineering and the Sciences, 4th ed., Prentice-Hall, New Jersey, 1995.